2021

True gravity in ocean dynamics Part 1 Ekman transport

Chu, Peter C.

Elsevier

Chu, Peter C. "True gravity in ocean dynamics Part 1 Ekman transport." Dynamics of Atmospheres and Oceans 96 (2021): 101268.
http://hdl.handle.net/10945/68909

Dynamics of Atmospheres and Oceans 96 (2021) 101268

Contents lists available at ScienceDirect

Dynamics of Atmospheres and Oceans

journal homepage: www.elsevier.com/locate/dynatmoce

True gravity in ocean dynamics Part 1 Ekman transport

Peter C. Chu

Department of Oceanography, Naval Postgraduate School, 1 University Circle, Monterey, CA 93943, USA

ARTICLE INFO

Keywords:
True gravity
Standard gravity
Deflected-vertical
Ekman spiral
Ekman transport
E-number

ABSTRACT

The direction normal to the Earth spherical (or ellipsoidal) surface is not vertical (called deflected vertical) since the vertical direction is along the true gravity $\mathbf{g}$ ($= \mathbf{i}g_\lambda + \mathbf{j}g_\varphi + \mathbf{k}g_z$). Here, ($\lambda$, φ, z) are (longitude, latitude, depth), and ($\mathbf{i}$, $\mathbf{j}$, $\mathbf{k}$) are the corresponding unit vectors. The spherical (or ellipsoidal) surfaces are not horizontal surfaces (called deflected-horizontal surfaces). The most important body force $\mathbf{g}$ (true gravity) has been greatly simplified without justification in oceanography to the standard gravity ($-g_0\mathbf{k}$) with $g_0 = 9.81$ m/s^2. Impact of such simplification on ocean dynamics is investigated in this paper using the Ekman layer model. In the classical Ekman layer dynamic equation, the standard gravity ($-g_0\mathbf{k}$) is replaced by the true gravity $\mathbf{g}(\lambda, \varphi, z)$ with a constant eddy viscosity and a depth-dependent-only density $\rho(z)$ represented by an e-folding near-inertial buoyancy frequency. New Ekman spiral and in turn new formulae for the Ekman transport are obtained for ocean with and without bottom. With the gravity data from the global static gravity model EIGEN-6C4 and the surface wind stress data from the Comprehensive Ocean-Atmosphere Data Set (COADS), large difference is found in the Ekman transport using the true gravity and standard gravity.

1. Introduction

If the Earth is assumed to be a rigid sphere with uniform mass distribution and without rotation, the gravity exerted on the ocean particle from this spherical Earth is a single-directional vector

$$\mathbf{g}_S = -g_0\mathbf{k}, \quad g_0 = 9.81\text{ms}^{-2} \tag{1}$$

where g_0 is called the standard gravity; $\mathbf{k}$ is the unit vector perpendicular to the spherical surface (upward positive). The corresponding standard geopotential (i.e., negation of the *standard gravity* potential) (Φ_0) is given by

$$\Phi_0(z) = g_0 z, \quad \mathbf{g}_S = -\frac{d\Phi_0}{dz}\mathbf{k} \tag{2}$$

Usually the polar spherical coordinate system (λ, φ, z) is used with the standard gravity with λ the longitude, φ the latitude, and z the depth.

If the uniform spherical Earth rotates, it becomes an ellipsoid. The theoretical Earth is this ellipsoid with the same total Earth mass and angular velocity, as well as coinciding its minor axis with the Earth's mean rotation (Vaníček and Krakiwsky, 1986). The gravity exerted on the ocean particle from this theoretical Earth is also a single-directional vector

E-mail address: pcchu@nps.edu.

https://doi.org/10.1016/j.dynatmoce.2021.101268
Received 20 August 2021; Received in revised form 14 October 2021; Accepted 25 October 2021
Available online 29 October 2021

$$\mathbf{g}_N = -g(\varphi)\mathbf{K} \tag{3}$$

where $\mathbf{g}_N$ is the sum of the gravitational and centrifugal accelerations, and called the theoretical/normal gravity in geodetic community (Cassinis, 1930) and the effective gravity in meteorological and oceanographic community (Vallis, 2006); $\mathbf{K}$ is the unit vector perpendicular to the ellipsoidal surface (upward positive). Its intensity $g(\varphi)$ is called the normal gravity and determined analytically. For example, the World Geodetic System 1984 uses the Somiglina equation (National Geospatial-Intelligence Agency, 1984) to represent $g(\varphi)$

$$g(\varphi) = g_e\left[\frac{1+\kappa\sin^2\varphi}{\sqrt{1-e^2\sin^2\varphi}}\right], e^2 = \frac{a^2-b^2}{a^2},\ \kappa = \frac{bg_p - ag_e}{ag_e} \tag{4}$$

where (a, b) are the equatorial and polar semi-axes; a is used for the Earth radius, $R = a = 6.3781364 \times 10^6$ m; $b = 6.3567523 \times 10^6$ m; e is the spheroid's eccentricity; $g_e = 9.780$ m/s^2, is the gravity at the equator; and $g_p = 9.832$ m/s^2 is the gravity at the poles. The corresponding normal geopotential (Φ_N) is given by

$$\Phi_N(z) = g(\varphi)z,\ \ \mathbf{g}_N = -\frac{\partial\Phi_N}{\partial z}\mathbf{K} \tag{5}$$

Usually the oblate spheroid coordinate system is used with the normal gravity. It shares the same longitude (λ) with the polar spherical coordinate system but different latitude (φ_{ob}) and radial coordinate (representing the deflected vertical) (z_{ob}). Note that the maximum error between using the oblate spheroid and polar spherical coordinates is about 0.17% (Gill, 1982). However, the dynamical error may be larger (Vallis, 2006). The polar spherical coordinate system is generally used in oceanography as well in geodesy, i.e., the unit vector $\mathbf{K}$ is represented approximately by $\mathbf{k}$. Both standard gravity $\mathbf{g}_S$ and normal gravity $\mathbf{g}_N$ don't have latitudinal and longitudinal components.

With rotation and non-uniform mass distribution, the gravity exerted on the ocean particle from the true Earth, called the true gravity ($\mathbf{g}$), is a three-dimensional vector field,

$$\mathbf{g}(\lambda,\varphi,z) = -g(\varphi)\mathbf{k} + \delta\mathbf{g}(\lambda,\varphi,z) \tag{6}$$

where $\delta\mathbf{g}$ is the gravity disturbance (Hackney and Featherstone, 2003). The corresponding potential of the gravity disturbance (called the disturbing gravity potential) is given by

$$\delta\mathbf{g} = \nabla_3 T(\lambda,\varphi,z) \tag{7}$$

where

$$\nabla_3 = \mathbf{i}\frac{1}{R\cos\varphi}\frac{\partial}{\partial\lambda} + \mathbf{j}\frac{1}{R}\frac{\partial}{\partial\varphi} + \mathbf{k}\frac{\partial}{\partial z} \tag{8}$$

is the three-dimensional vector differential operator; and $R = 6.3781364 \times 10^6$ m, is the Earth radius. Substitution of (7) into (6) leads to

$$\mathbf{g}(\lambda,\varphi,z) = \mathbf{g}_h + g_z\mathbf{k},\ \ \mathbf{g}_h \equiv (g_\lambda, g_\varphi) = \nabla T,\ \ g_z = \frac{\partial T}{\partial z} - g(\varphi) \tag{9}$$

where $\nabla \equiv \mathbf{i}\frac{\partial}{R\cos\varphi\partial\lambda} + \mathbf{j}\frac{\partial}{R\partial\varphi}$ is the two-dimensional vector differential operator; $\mathbf{g}_h$ is the latitudinal (g_φ) and longitudinal (g_λ) gravity component; and $g_z\mathbf{k}$ is the component in the direction of $\mathbf{k}$. Since the deviation of the deflected-vertical component of the gravity (g_z) to the constant (-g_0) is around 4 orders of magnitude smaller than g_0, it leads to

$$g_z \approx -g_0 \tag{10}$$

Substitution of (10) into (9) leads to

$$\mathbf{g}(\lambda,\varphi,z) \approx \mathbf{g}_h - g_0\mathbf{k} \tag{11}$$

for oceanography.

The spherical expansion of the disturbing static gravity potential (T) in the polar spherical coordinates outside the Earth masses is given by (Kostelecký et al., 2015)

$$T\left(\lambda,\varphi,z\right) = \frac{GM}{(R+z)}\sum_{l=2}^{\infty}\sum_{m=0}^{l}\left(\frac{R}{R+z}\right)^l\left[\left(C_{l,m} - C_{l,m}^{el}\right)\cos m\lambda + S_{l,m}\sin m\lambda\right]P_{l,m}\left(\sin\varphi\right), \tag{12}$$

where $M = 5.9736 \times 10^{24}$ kg, is the mass of the Earth; $G = 6.674 \times 10^{-11}$ m^3 kg^{-1} s^{-2}, is the gravitational constant; ($C_{l,m}$,$C_{l,m}^{el}$,$S_{l,m}$) are the harmonic geopotential coefficients with $C_{l,m}^{el}$belonging to the reference ellipsoid; and $P_{l,m}(\sin\varphi)$are the Legendre associated functions with (l, m) the degree and order of the harmonic expansion. According to (12), the ratio between $T(\lambda, \varphi, z)$ to $T(\lambda, \varphi, 0)$

through the water column can be roughly estimated by

$$\left|\frac{T(\lambda,\varphi,z)}{T(\lambda,\varphi,0)}\right| \approx \frac{R}{(R+z)} \approx 1, \quad 0 \geq z \geq -H(\lambda,\varphi) \tag{13}$$

where H is the water depth. Since the Earth radius (R) is more than 3 orders of magnitude larger than the water depth H, the surface disturbing gravity potential $T(\lambda, \varphi, 0)$ is used for the whole water column,

$$T(\lambda,\varphi,z) \approx T(\lambda,\varphi,0), 0 \geq z \geq -H(\lambda,\varphi) \tag{14}$$

Also, the surface disturbing gravity potential $T(\lambda, \varphi, 0)$ is related to the geoid height (N) by the Bruns' formula (Sandwell and Smith, 1997)

$$N\left(\lambda,\varphi\right) = \frac{T(\lambda,\varphi,0)}{g_0} \tag{15}$$

Substitution of (14) into the second equation in (9) and use of (15) lead to

$$\mathbf{g}_h(\lambda,\varphi,z) = \nabla T(\lambda,\varphi,0) = g_0 \nabla N \tag{16}$$

which shows the independence of $\mathbf{g}_h$ on z for the whole water column. With approximations (11) and (14), the true geopotential is given by (Vaníček and Krakiwsky, 1986)

$$\Phi = \Phi_0 - T \approx \Phi_0 - g_0 N(x,y)$$

which hasn't been recognized in the oceanographic community.

The Earth true gravity ($\mathbf{g}$) represents the vertical direction. The true geopotential surfaces such as the geoid surface are the horizontal surfaces. The angle between (-$\mathbf{k}$) and $\mathbf{g}$ is called the vertical deflection. The ocean dynamics has been established with the deflected-vertical coordinate system using the standard gravity (mostly) and the normal gravity (very few) and never using the true gravity $\mathbf{g}(\lambda, \varphi, z)$.

The seminal paper by Ekman (1905) laid the foundation for the modern oceanography through modeling the turbulent mixing in upper ocean as a diffusion process similar to molecular diffusion, with an eddy viscosity K, which was taken as a constant with many orders of magnitude larger than the molecular viscosity. The Ekman theory was established using the standard gravity ($-g_0\mathbf{k}$). The turbulent mixing generates ageostrophic component of the upper ocean currents (called the Ekman spiral), decaying by an e-folding over a depth as the current vector rotate to the right (left) in the northern (southern) hemisphere through one radian. Along with the Ekman spiral, the Ekman transport was identified. Recent research (Chu, 2021) show that the latitudinal-longitudinal true gravity component $\mathbf{g}_h$ ($= g_\lambda \mathbf{i} + g_\varphi \mathbf{j}$) is comparable to the horizontal pressure gradient force, Coriolis force, and surface wind stress. Thus, the feasibility to neglect $\mathbf{g}_h$ in the ocean Ekman layer dynamics needs to be investigated. In this study, the additional forcing $\mathbf{g}_h$ is added to the classical Ekman dynamic equation and new formulas for the Ekman spiral and transport are obtained.

The rest of the paper are outlined as follows. Section 2 presents the basic equation with the true gravity $\mathbf{g}(\lambda, \varphi, z)$ for the Ekman dynamics. Section 3 lists the model parameters. Sections 4–5 show the Ekman spiral and transport with the true gravity. Section 6 describes the two datasets used for this study. Sections 7–8 present the global Ekman transport without and with bottom. The non-dimensional E and E^*numbers are calculated from the geoid and surface wind stress data and show the importance of $\mathbf{g}_h$. Section 9 depicts the difference between the true-vertical and deflected-vertical coordinate systems. Section 10 presents the conclusions.

2. Dynamic equation with the true gravity

Steady-state large-scale ocean dynamic equation with the Boussinesq approximation (replacing density ρ by a constant ρ_0 except ρ being multiplied by the gravity) is given by

$$\rho_0[2\boldsymbol{\Omega} \times \mathbf{U}] = -\nabla_3 p + \rho \mathbf{g} + \rho_0 \mathbf{F} \tag{17}$$

if the pressure gradient force, gravity, and friction are the only real forces (Chu, 2021). Here, $\mathbf{U} = (u_\lambda, u_\varphi)$, is the two-dimensional velocity vector; $\boldsymbol{\Omega} = \Omega(\mathbf{j}\cos\varphi + \mathbf{k}\sin\varphi)$, is the Earth rotation vector with $\Omega = 2\pi/(86{,}164\text{ s})$ the Earth rotation rate; ρ is the density; $\rho_0 = 1028\text{ kg/m}^3$, is the characteristic density; p is the pressure; $\mathbf{F}$ is turbulent diffusive force due to the Earth radial shear represented by

$$\mathbf{F} = \frac{\partial}{\partial z}\left(K\frac{\partial \mathbf{U}}{\partial z}\right) \tag{18}$$

Traditionally, the deflected-horizontal velocity $\mathbf{U}$ is decomposed into geostrophic and Ekman (ageostrophic) velocities,

$$\mathbf{U} = \mathbf{U}_g + \mathbf{U}_E, \quad \rho_0\left[2\boldsymbol{\Omega} \times \mathbf{U}_g\right] = -\nabla p \tag{19}$$

where $\mathbf{U}_E = (u_E, v_E)$ is the Ekman velocity vector. After substitution of (11), (18), and (19) into (17), the deflected-horizontal component of (17) is represented by

$$\rho_0[2\boldsymbol{\Omega}\times\mathbf{U}_E]=\rho\mathbf{g}_h+\rho_0\frac{\partial}{\partial z}\left(K\frac{\partial\mathbf{U}_E}{\partial z}\right)+\rho_0\frac{\partial}{\partial z}\left(K\frac{\partial\mathbf{U}_g}{\partial z}\right) \tag{20}$$

Baroclinicity (i.e., non-zero deflected-horizontal density gradient) and spatially varying eddy viscosity K affect the Ekman layer dynamics (Chu, 2015). To limit the study on the effect of $\mathbf{g}_h$ only, the eddy viscosity K is assumed constant and the density varies in the z-direction only, i.e., there is no deflected-vertical shear of the geostrophic current

$$\partial\mathbf{U}_g/\partial z=0. \tag{21}$$

Furthermore, a special density stratification is selected for this study as the e-folding near-inertial buoyancy frequency (Garrett, 2001),

$$\Theta(z)=\Theta_0\exp\left(\frac{z}{d}\right),\Theta^2(z)\equiv-\frac{g_0}{\rho_0}\frac{d\widetilde{\rho}}{dz} \tag{22a}$$

where $\widetilde{\rho}$ is the density anomaly relative to ρ_0; and d is the e-folding depth of $\Theta(z)$, which represents the dependence of the density with z. The second formula in (22a) becomes

$$ds(z)\Big/dz=-\frac{\Theta_0^2}{g_0}e^{2z/d},s(z)\equiv1+\widetilde{\rho}\Big/\rho_0=1-\frac{\Theta_0^2d}{2g_0}e^{2z/d} \tag{22b}$$

Substitution of (21) and (22b) into (20) leads to the Ekman dynamic equation including $\mathbf{g}_h$

$$2\boldsymbol{\Omega}\times\mathbf{U}_E=s(z)\mathbf{g}_h+K\frac{\partial^2\mathbf{U}_E}{\partial z^2} \tag{23}$$

which shows that $\mathbf{g}_h$ can also generate deflected-vertical shear (i.e., the Ekman spiral) without surface winds if the density varies with z.

Let the deflected-horizontal gravity component ($\mathbf{g}_h$), Ekman velocity ($\mathbf{U}_E$) be represented in complex variables

$$G_h=g_\lambda+ig_\varphi,\quad U=u_E+iv_E,i\equiv\sqrt{-1} \tag{24}$$

The Ekman Eq. (23) is converted into the complex form

$$\frac{\partial^2U}{\partial z^2}-i\frac{f}{K}U=-\frac{G_h}{K}s(z). \tag{25}$$

The turbulent momentum flux should be continuous at the ocean surface ($z=0$),

$$\rho_0K\frac{\partial U}{\partial z}|_{z=0}=\tau_\lambda^{(w)}+i\tau_\varphi^{(w)} \tag{26}$$

where $(\tau_\lambda^{(w)},\tau_\varphi^{(w)})$ are the surface wind stress components. Two types of the Ekman velocity are considered. The first one is the typical Ekman spiral with no bottom. Its lower boundary condition is given as,

$$|U|\to0\ \text{ as z}\to-\infty \tag{27a}$$

The second one is with bottom (z = -H). Its lower boundary condition is given by,

$$\rho_0K\frac{\partial U*}{\partial z}|_{z=-H}=\tau_\lambda^{(b)}+i\tau_\varphi^{(b)} \tag{27b}$$

where $(\tau_\lambda^{(b)},\tau_\varphi^{(b)})$are the bottom frictional stress components; H (= 4000 m) is the water depth. The purpose to introduce the second type is to show the effect of bottom friction on the Ekman velocity. The linear relation is used for the bottom frictional stress

$$\tau_\lambda^{(b)}+i\tau_\varphi^{(b)}=-\gamma\rho_0U*(-H) \tag{28}$$

where γ is the bottom friction coefficient. Integration with respect to z of U (or U*) from -∞ (-H) to 0 leads to the two types of the Ekman transport

$$M=\rho_0\int_{-\infty}^{0}Udz,\quad M*=\rho_0\int_{-H}^{0}U*dz \tag{29}$$

3. Model parameters

This Ekman model has four parameters with (Θ_0, d) for the density stratification, γ for the bottom friction coefficient, and K for the eddy viscosity. Let

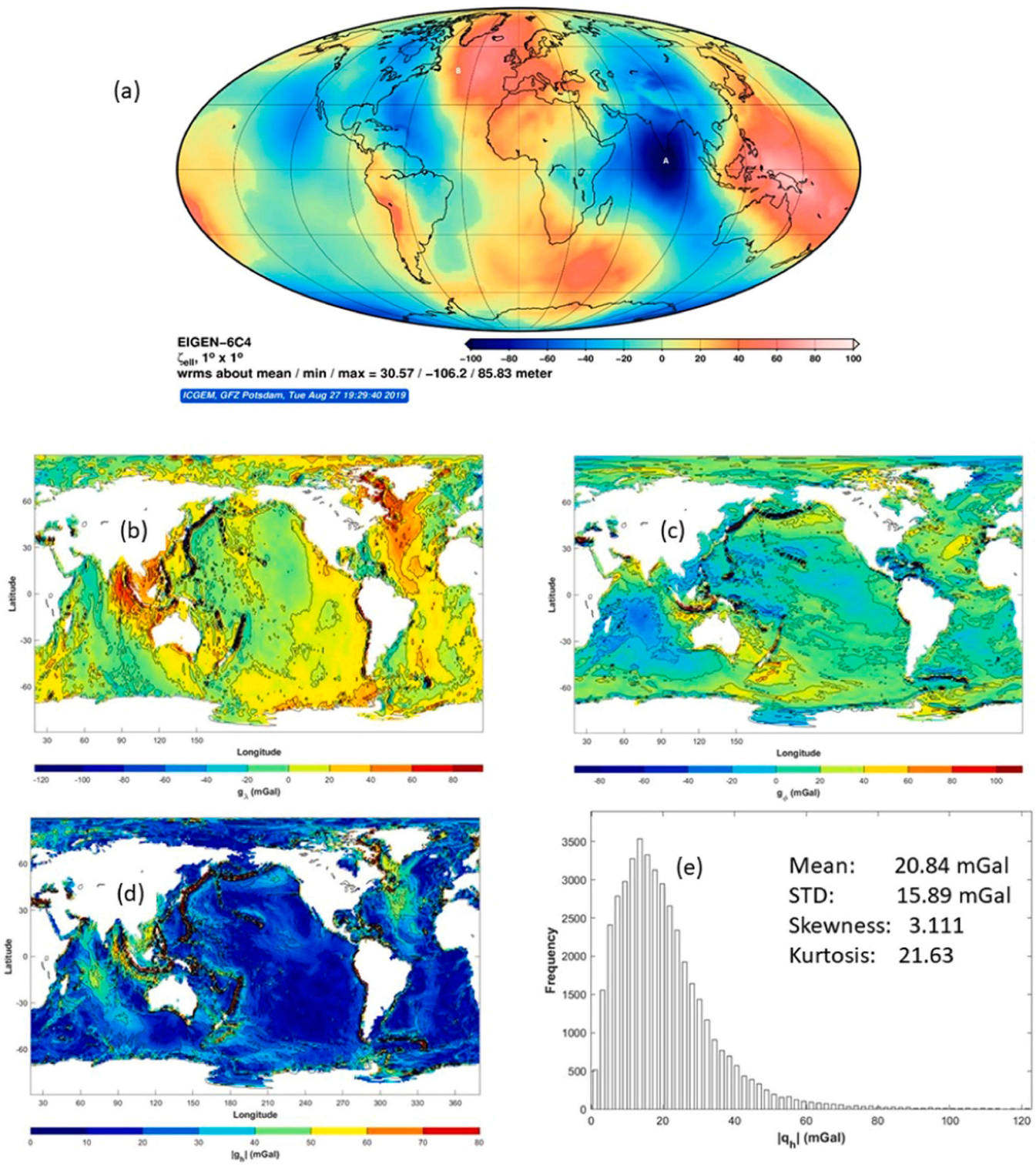

Fig. 1. Horizontal gravity components (unit: mGal) at z = 0 from the EIGEN-6C4 geoid height (N): (a) digital data of N with $1^\circ \times 1^\circ$, computed online at the website http://icgem.gfz-potsdam.de/home, (b) longitudinal component (g_λ), (c) latitudinal component (g_φ), (d) contour plot of $|\mathbf{g}_h|$, and (e) histogram of $|\mathbf{g}_h|$ (from Figs. 1 and 2 in Chu, 2021, https://www.nature.com/articles/s41598-021–82882-1).

$$D_E \equiv \pi\sqrt{\frac{2K}{|f|}},\ \chi \equiv \frac{D_E}{\pi d} = \frac{\sqrt{2K/|f|}}{d},\ A \equiv \frac{\gamma D_E}{2\pi K},\ B \equiv \frac{\rho_0 \Theta_o^2 D_E^2}{2\pi^2(4\chi^4+1)} \tag{30}$$

Here, D_E is the Ekman layer depth; χ is proportion to the ratio between the Ekman layer depth (D_E) and the e-folding depth (d) of the buoyancy frequency; A is the ratio between the bottom friction coefficient and eddy viscosity; B represents the strength of the deflected-horizontal gravity component on the Ekman flow. The eddy viscosity K was estimated from observations varying from 0.054 $m^2\ s^{-1}$ in the western Sargasso Sea (34°N, 70°W) during the summer of 1982 (Price et al., 1987), to 0.006 $m^2\ s^{-1}$ in the Strait of Georgia, British Columbia (Stacey et al., 1986). The smaller value (0.006 $m^2\ s^{-1}$) may be treated as a lower bound of the eddy viscosity (Price et al., 1987). The other three parameters are given by

$$\Theta_0 = 2.56 \times 10^{-3} s^{-1},\ d\ = 1.3 km,\ \gamma\ = 4 \times 10^{-6} ms^{-1} \tag{31}$$

where the parameter Θ_0 is estimated from (King et al., 2012). The parameter d is obtained from (Garrett, 2001). The parameter γ is determined as 2.34 $\times\ 10^{-5}$ m s^{-1} for the Hudson Bay from SEASAT-ALT data (Moon and Tang, 1987). The area-integrated dissipations for various regions of the global oceans show that the Hudson Bay has the maximum value (>250 GW), which is around 5–6 times as large as the other areas (see Fig. 2 in Egbert and Ray, 2000). Thus, γ is taken as 4 $\times\ 10^{-6}$ m s^{-1} in this study. With the larger value of K = 0.054 $m^2\ s^{-1}$, the Ekman layer thickness D_E, ratio A, and parameter χ are estimated by

$$D_E = \frac{0.06582}{\sqrt{|\sin\varphi|}}d,\ \chi = \frac{\sqrt{2K/|f|}}{d} = \frac{0.02095}{\sqrt{|\sin\varphi|}},\ \ A = \frac{1.425 \times 10^{-3}}{\sqrt{\sin|\varphi|}}. \tag{32}$$

Here, D_E varies from 289 m at φ = 5° (N or S) to 86 m at φ = 90° (N or S); the parameter χ varies from 0.071 at φ = 5° (N or S) to 0.021 at φ = 90° (N or S); and A varies from 4.827 $\times\ 10^{-3}$ at φ = 5° (N or S) to 1.42510^{-3} at φ = 90° (N or S). The maximum values of A, $\chi^2$and χ^4(at φ = 5° S or N) are small

$$A \le 4.827 \times 10^{-3},\ \chi^2 \le 0.5036 \times 10^{-2},\ \chi^4 \le 0.2536 \times 10^{-4} \tag{33}$$

which are even smaller if the value of K smaller than 0.054 $m^2\ s^{-1}$.

4. Ekman solution in complex form

Eq. (25) with the boundary conditions (26) and (27a) has the exact solution

$$\begin{aligned} U(z) = {} & \frac{D_E}{2\pi\rho_0 K}\left\{\left(\tau_\lambda + \tau_\varphi\right) + i\left(\tau_\varphi - \tau_\lambda\right) - BG_h\left[\left(2\chi^2+1\right) - i\left(2\chi^2-1\right)\right]\right\}e^{(1+i)\pi z/D_E} \\ & + \frac{BdG_h}{2\rho_0 K}\left(2\chi^2 + i\right)e^{2z/d} \end{aligned} \tag{34}$$

and the corresponding Ekman transport without bottom is given by

$$M = \rho_0\int_{-\infty}^{0} U dz = \frac{1}{f}\left(\tau_\varphi - i\tau_\lambda\right) - \frac{BG_h}{f}\left(1 - i2\chi^2\right) + \frac{d^2 BG_h}{4K}\left(2\chi^2 + i\right) \tag{35}$$

Similarly, Eq. (25) with the boundary conditions (26) and (27b) has the exact solution

$$\begin{aligned} U*(z) = {} & \frac{D_E}{2\pi\rho_0 K}\left\{\left(\tau_\lambda^{(w)} + \tau_\varphi^{(w)}\right) + i\left(\tau_\varphi^{(w)} - \tau_\lambda^{(w)}\right) - BG_h\left[\left(2\chi^2+1\right) - i\left(2\chi^2-1\right)\right]\right\}e^{(1+i)\pi z/D_E} \\ & - \frac{D_E}{2\pi\rho_0 K}\left[\left(\tau_\lambda^{(b)} + \tau_\varphi^{(b)}\right) + i\left(\tau_\varphi^{(b)} - \tau_\lambda^{(b)}\right)\right]e^{-(1+i)\pi(z+H)/D_E} + \frac{BdG_h}{2\rho_0 K}\left(2\chi^2 + i\right)e^{2z/d} - i\frac{G_h}{f} \end{aligned} \tag{36}$$

where the following inequalities are used

$$\left|e^{-(1+i)\pi H/D_E}\right| \ll 1, e^{-2H/d} \ll 1 \tag{37}$$

Evaluation of (36) at the ocean bottom (z = -H) and use of (37) give

$$U*\left(-H\right) = -\frac{D_E}{2\pi\rho_0 K}\left[\left(\tau_\lambda^{(b)} + \tau_\varphi^{(b)}\right) + i\left(\tau_\varphi^{(b)} - \tau_\lambda^{(b)}\right)\right] - i\frac{G_h}{f} \tag{38}$$

Substitution of (38) into (28) leads to

$$\tau_\lambda^{(b)} + i\tau_\varphi^{(b)} = \gamma\frac{D_E}{2\pi K}\left[\left(\tau_\lambda^{(b)} + \tau_\varphi^{(b)}\right) + i\left(\tau_\varphi^{(b)} - \tau_\lambda^{(b)}\right)\right] + i\gamma\rho_0\frac{G_h}{f} \tag{39}$$

which is re-arranged as a set of two linear algebraic equations

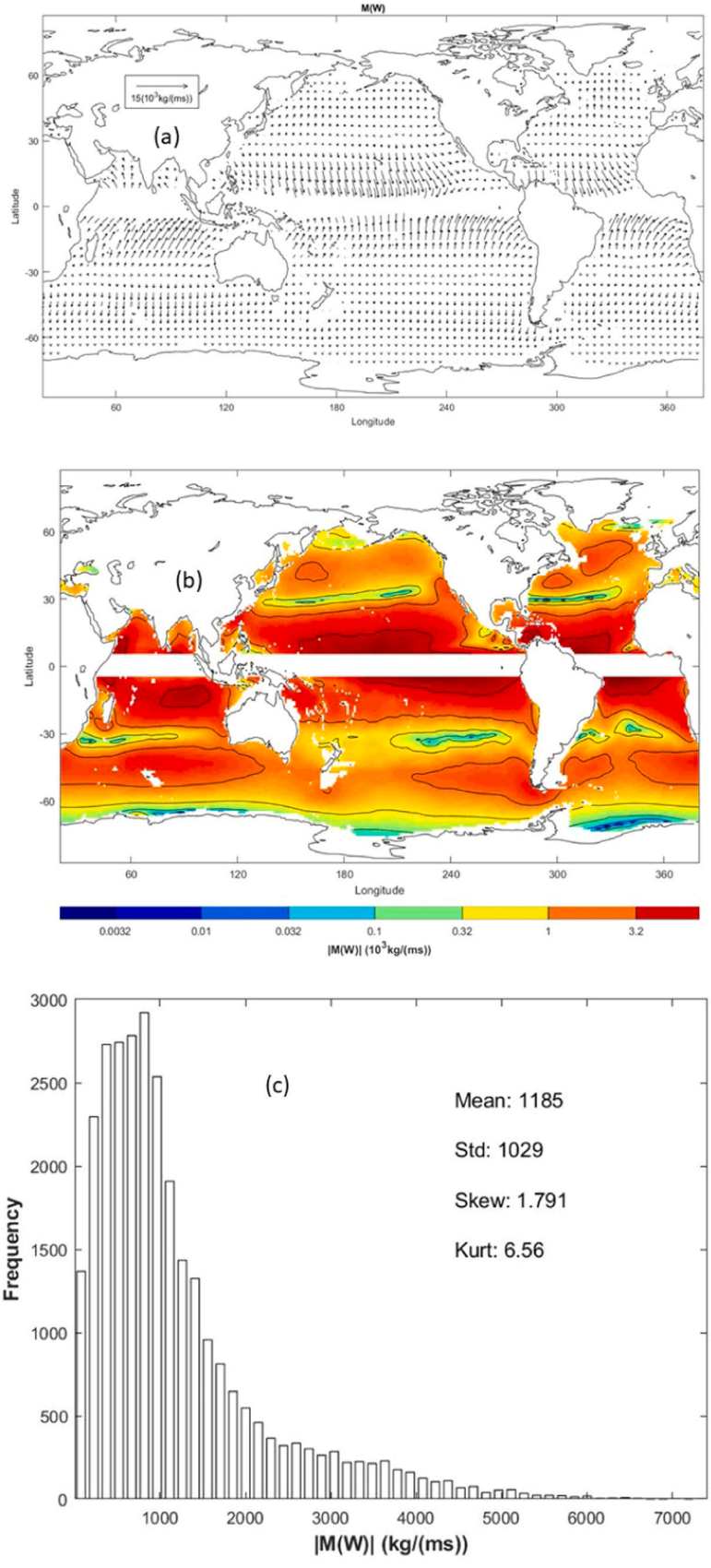

(caption on next page)

Fig. 2. Climatological annual mean Ekman transport due to surface wind stress $\mathbf{M}_w$ (unit: kg $m^{-1}s^{-1}$) calculated using the COADS data: (a) vector plot of $\mathbf{M}_w$, (b) contour plot of $|\mathbf{M}_w|$, and (c) histogram of $|\mathbf{M}_w|$.

$$A\left(\tau_\lambda^{(b)}+\tau_\varphi^{(b)}\right)-\tau_\lambda^{(b)}=\frac{\gamma\rho_0}{f}g_\varphi \tag{40}$$

$$A\left(\tau_\varphi^{(b)}-\tau_\lambda^{(b)}\right)-\tau_\varphi^{(b)}=-\frac{\gamma\rho_0}{f}g_\lambda \tag{41}$$

Since $A \le 4.827\times10^{-3}$[see (33)], Eqs. (40) and (41) can be simplified further into

$$\tau_\lambda^{(b)}=-\frac{\gamma\rho_0}{f}g_\varphi,\ \tau_\varphi^{(b)}=\frac{\gamma\rho_0}{f}g_\lambda \tag{42}$$

Substitution of (42) into (36) and use of (33) [i.e., small parameter χ^2] lead to

$$\begin{aligned}U*(z)=&\frac{D_E}{2\pi\rho_0K}\left\{\left(\tau_\lambda^{(w)}+\tau_\varphi^{(w)}\right)+i\left(\tau_\varphi^{(w)}-\tau_\lambda^{(w)}\right)-BG_h[(1+i)]\right\}e^{(1+i)\pi z/D_E}\\&-\frac{D_E}{2\pi K}\frac{\gamma}{f}[(-g_\varphi+g_\lambda)+i(g_\lambda+g_\varphi)]e^{-(1+i)\pi(z+H)/D_E}+\frac{BdG_h}{2\rho_0K}ie^{2z/d}-i\frac{G_h}{f}\end{aligned} \tag{43}$$

where B is simplified as

$$B=\frac{\rho_0\Theta_o^2D_E^2}{2\pi^2} \tag{44}$$

The last term in (43), $-iG_h/f$, represents the effect of $\mathbf{g}_h$ on the currents, but does not vary with z. We may not consider it as part of the Ekman spiral. Integration of (43) with respect to z from $-H$ to 0 without the term ($-iG_h/f$) leads to the complex form of the Ekman transport with bottom

$$\begin{aligned}M*=&\rho_0\int_{-H}^{0}\left(U+i\frac{G_h}{f}\right)dz=\frac{1}{f}\left[\tau_\varphi^{(w)}-i\tau_\lambda^{(w)}-BG_h\right]\left[1-e^{-(1+i)\pi H/D_E}\right]\\&+\frac{\rho_0}{|f|}\frac{\gamma}{f}G_h\left[e^{-(1+i)\pi H/D_E}-1\right]+\frac{d^2BG_h}{4K}i\left[1-e^{-2H/d}\right]\end{aligned} \tag{45}$$

which is simplified after using (37) and (44)

$$M*=\frac{1}{f}\left[\tau_\varphi^{(w)}-i\tau_\lambda^{(w)}\right]-\frac{\rho_0}{|f|f}\left(\gamma+\frac{\Theta_o^2K}{g_0}\right)G_h+i\frac{\rho_0\Theta_0^2d^2}{4fg_0}G_h \tag{46}$$

With $\Theta_0=2.56\times10^{-3}s^{-1}$, and$K=0.054m^2s^{-1}$, the term $\Theta_o^2K/g_0(=3.61\times10^{-8}\ m\ s^{-1})$ is two orders of magnitude smaller than γ ($4\times10^{-6}\ m\ s^{-1}$) and therefore can be neglected. Thus, Eq. (46) becomes

$$M*=\frac{1}{f}\left[\tau_\varphi^{(w)}-i\tau_\lambda^{(w)}\right]-\frac{\rho_0\gamma}{|f|f}G_h+i\frac{\rho_0\Theta_0^2d^2}{4fg_0}G_h \tag{47}$$

5. New formulae for the Ekman transports

The Ekman transports (35) and (47) are transformed back into the vector forms

$$\mathbf{M}=-\mathbf{k}\times\frac{\boldsymbol{\tau}}{f}+\left(\frac{\rho_0\Theta_0^2d^2}{4fg_0}\right)\mathbf{k}\times\mathbf{g}_h-\frac{\rho_0\Theta_o^2K}{f|f|g_0}\mathbf{g}_h \tag{48}$$

which shows the contribution of $\mathbf{g}_h$ to the Ekman transport without bottom, and

$$\mathbf{M}*=-\mathbf{k}\times\frac{\boldsymbol{\tau}}{f}+\left(\frac{\rho_0\Theta_0^2d^2}{4fg_0}\right)\mathbf{k}\times\mathbf{g}_h-\frac{\rho_0\gamma}{f|f|}\mathbf{g}_h \tag{49}$$

which shows the contribution of $\mathbf{g}_h$ to the Ekman transport with bottom. Let the Ekman transports $\mathbf{M}$ and $\mathbf{M}^*$ be separated into two parts

$$\mathbf{M}=\mathbf{M}_W+\mathbf{M}_G,\mathbf{M}*=\mathbf{M}_W+\mathbf{M}_G^* \tag{50}$$

with

$$\mathbf{M}_W = -\mathbf{k}\times\frac{\boldsymbol{\tau}}{f} \tag{51}$$

due to the surface wind stress $\boldsymbol{\tau}$ (i.e., classical Ekman transport), and

$$\mathbf{M}_G = \mathbf{k}\times\frac{1}{f}\left(\frac{\rho_0\Theta_0^2 d^2}{4g_0}\mathbf{g}_h\right) - \frac{\rho_0\Theta_o^2 K}{f|f|g_0}\mathbf{g}_h, \tag{52a}$$

due to $\mathbf{g}_h$ with no bottom, and

$$\mathbf{M}_G^* = \mathbf{k}\times\frac{1}{f}\left(\frac{\rho_0\Theta_0^2 d^2}{4g_0}\mathbf{g}_h\right) - \frac{\rho_0\gamma}{f|f|}\mathbf{g}_h, \tag{52b}$$

due to $\mathbf{g}_h$ with bottom. Both $\mathbf{M}_G$ and $\mathbf{M}_G^*$have along and across $\mathbf{g}_h$ components.

The ratio between the two components for $\mathbf{M}_G$ is given by

$$\frac{|\text{Along } \mathbf{g}_h|}{|\text{Across } \mathbf{g}_h|} = \frac{\left[\rho_0\Theta_o^2 K/(f|f|g_0)\right]\mathbf{g}_h}{\left[\left(\rho_0\Theta_0^2 d^2\right)/(4fg_0)\right]\mathbf{g}_h} = \frac{K}{4d^2|f|} = \frac{\chi^2}{8} \ll 1 \tag{53}$$

where (33) is used. Eq. (52a) becomes

$$\mathbf{M}_G \simeq \mathbf{k}\times\frac{1}{f}\left(\frac{\rho_0\Theta_0^2 d^2}{4g_0}\mathbf{g}_h\right) \tag{54}$$

Substitution of (16) into (54) and (52) leads to

$$\mathbf{M}_G = \mathbf{k}\times\frac{1}{f}\left(\frac{\rho_0\Theta_0^2 d^2}{4}\nabla N\right),\quad \mathbf{M}_G^* = \mathbf{M}_G - \frac{\rho_0 g_0\gamma}{f|f|}\nabla N \tag{55}$$

Nondimensional E and E * numbers are defined by

$$E \equiv \frac{|\mathbf{M}_G|}{|\mathbf{M}_W|},\quad E* \equiv \frac{|\mathbf{M}_G^*|}{|\mathbf{M}_W|} \tag{56}$$

to represent the relative importance of $\mathbf{g}_h$ versus surface wind stress ($\boldsymbol{\tau}$) on the Ekman transport. Note that both E and E*numbers are independent on the eddy viscosity K, but dependent on $\Theta_0^2 d^2$, ∇N, and $|\boldsymbol{\tau}|$. In addition, E* depends on γ too.

6. Data sources

Two datasets were used to identify importance of $\mathbf{g}_h$ on the Ekman layer dynamics are: (a) global static geoid undulation (N) dataset from the EIGEN-6C4 model (Kostelecký et al., 2015) (http://icgem.gfz-potsdam.de/home) for computing the deflected-horizontal gravity component $\mathbf{g}_h$, and (b) climatological annual mean surface wind stress (τ_λ, τ_φ) data from the Comprehensive Ocean-Atmosphere Data Set (COADS) (da Silva et al., 1994) (http://iridl.ldeo.columbia.edu/SOURCES/. DASILVA/. SMD94/. climatology/).

Fig. 1a shows the global geoid height $N(\lambda, \varphi)$ with $1^\circ\times 1^\circ$ resolution from the EIGEN-6C4 model (Chu, 2021). With the geoid height data (N) obtained from the EIGEN-6C4, $N(\lambda, \varphi)$, the deflected-horizontal gravity components g_λ and g_φ are computed using Eq. (16), as shown in Fig. 1b and c. The magnitude of the deflected-horizontal gravity vector $|\mathbf{g}_h|$ is shown in Fig. 1d. The histogram of $|\mathbf{g}_h|$ (Figure1e) indicates a positively skewed distribution with a long tail extending to values larger than 100 mGal (1 mGal $= 10^{-5}$ ms^{-2}). The statistical characteristics of $|\mathbf{g}_h|$ are 20.84 mGal as the mean, 15.89 mGal as the standard deviation, 3.11 as the skewness, and 21.63 as the kurtosis. The statistical estimate of the mean intensity of $|\mathbf{g}_h|$ (20.84 mGal) is coherent with the simple calculation of $|\mathbf{g}_h|_{\text{AB}}$ between points A and B (20.45 mGal).

With these two datasets, the climatological annual mean Ekman transport is calculated by (51) due to the surface wind stress ($\mathbf{M}_W$), by (52a) due to $\mathbf{g}_h$ with no bottom ($\mathbf{M}_G$), and by (52b) due to $\mathbf{g}_h$ with bottom ($\mathbf{M}_G^*$) for the global oceans except for the equatorial region (5°S – 5°N) where the geostrophic balance does not exist. In addition, the global E- and E*-numbers are also computed by (56).

7. Global Ekman transport with no bottom

The calculated global Ekman transport has different patterns due to wind stress $\mathbf{M}_W$ (Fig. 2a) and due to $\mathbf{g}_h$ with no bottom ($\mathbf{M}_G$) (Fig. 3a). The intensities of the Ekman transport components $|\mathbf{M}_W|$ (Fig. 2b) and $|\mathbf{M}_G|$ (Fig. 3b) have different deflected-horizontal distributions and strengths. The histogram of $|\mathbf{M}_W|$ (Fig. 2c) shows near Gamma distribution with the shape parameter of 1 and scale parameter of 2, and with the mean and standard deviation (946.8, 993.9) kg m^{-1}s^{-1}. However, the histogram of $|\mathbf{M}_G|$ (Fig. 3c) shows near Weibull distribution with the shape parameter of 1.5 and scale parameter of 10, and with the mean and standard deviation (4098, 5836) kg m^{-1}s^{-1}.

Much larger Ekman transport due to $\mathbf{g}_h$ with no bottom ($|\mathbf{M}_G|$) than due to the surface wind stress $|\mathbf{M}_W|$ is shown in the world ocean

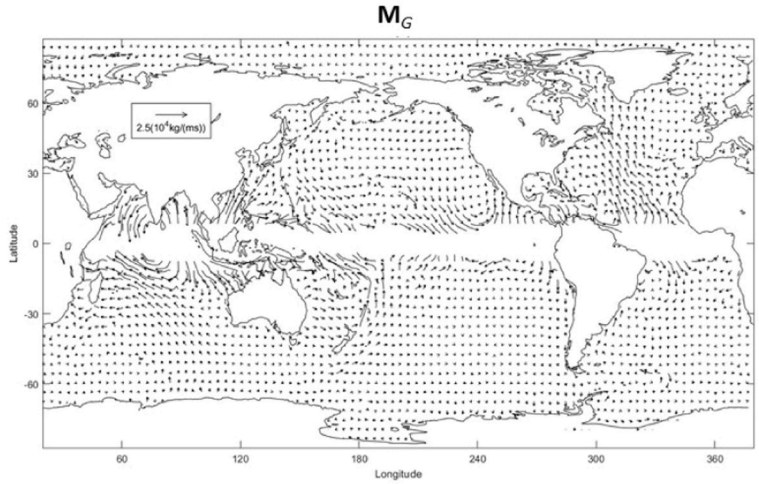

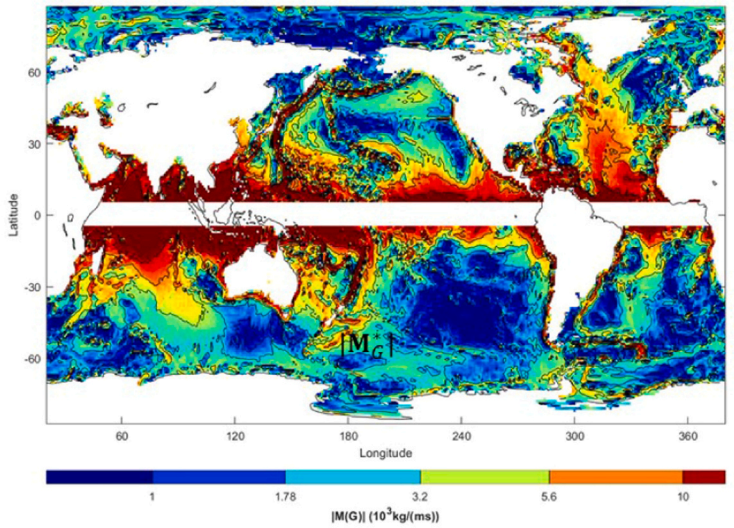

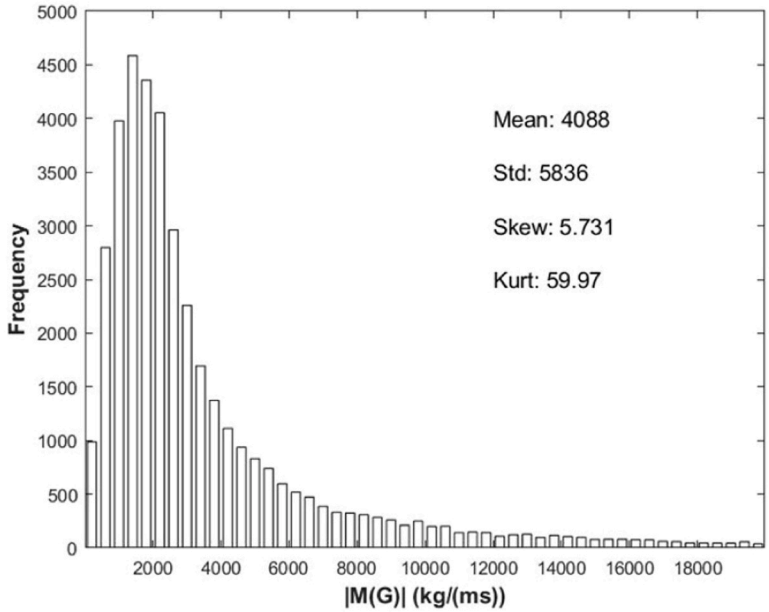

(caption on next page)

Fig. 3. Climatological annual mean Ekman transport due to $\mathbf{g}_h$ with no bottom ($\mathbf{M}_G$) (unit: kg m^{-1}s^{-1}) calculated using the EIGEN-6C4 geoid height (N) data: (a) vector plot of $\mathbf{M}_G$, (b) contour plot of $|\mathbf{M}_G|$, and (c) histogram of $|\mathbf{M}_G|$.

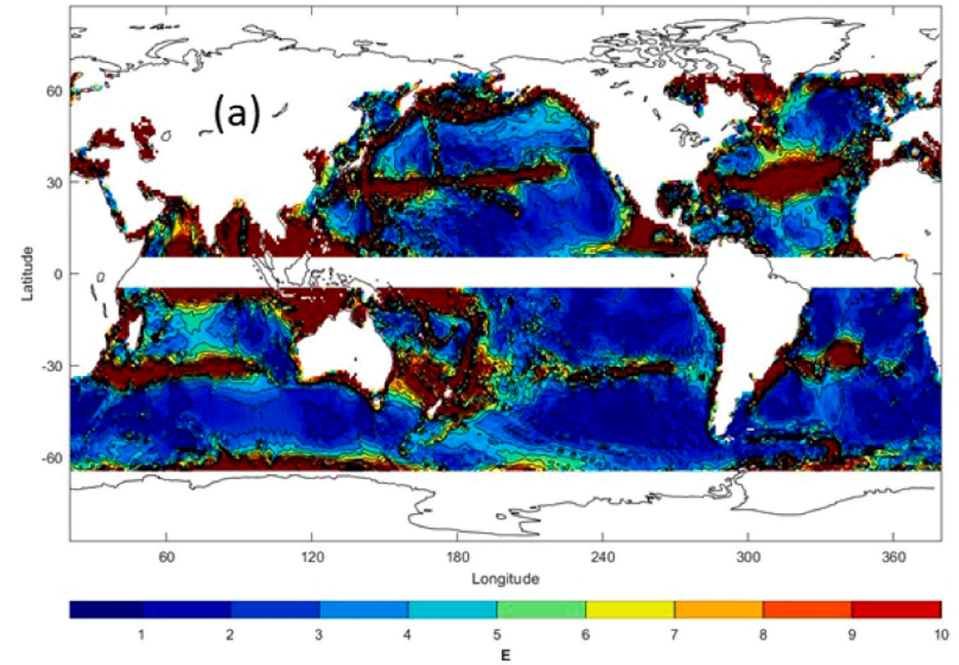

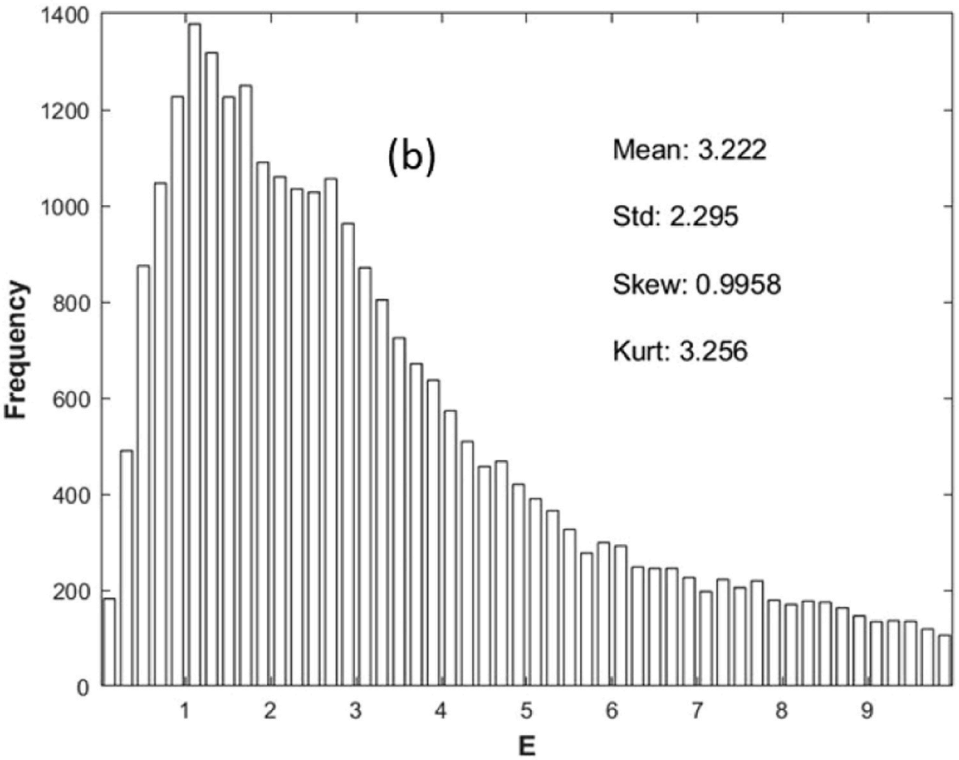

Fig. 4. Climatological annual mean non-dimensional E-number calculated using the COADS annual mean surface wind stress and the EIGEN-6C4 geoid undulation (N) data: (a) contour plot of E, (b) histogram of E.

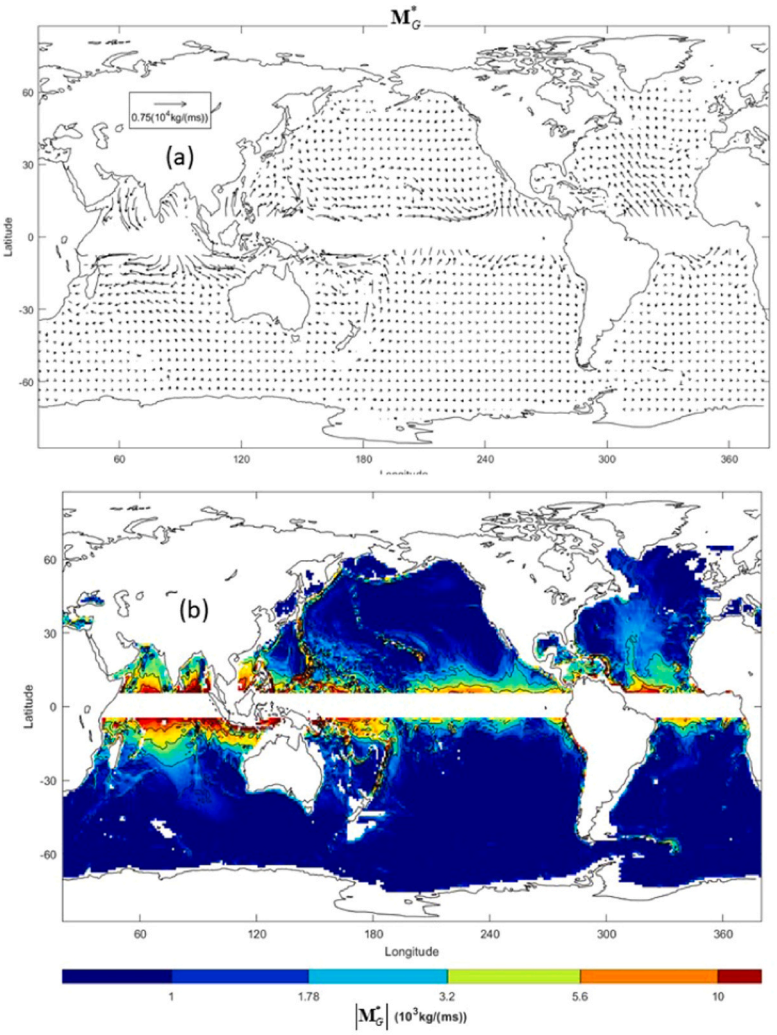

(caption on next page)

Fig. 5. Climatological annual mean Ekman transport due to $\mathbf{g}_h$ with bottom ($\mathbf{M}_G^*$) (unit: kg m^{-1}s^{-1}) calculated using the EIGEN-6C4 geoid height (N) data: (a) vector plot of $\mathbf{M}_G$, (b) contour plot of $|\mathbf{M}_G^*|$, and (c) histogram of $|\mathbf{M}_G^*|$.

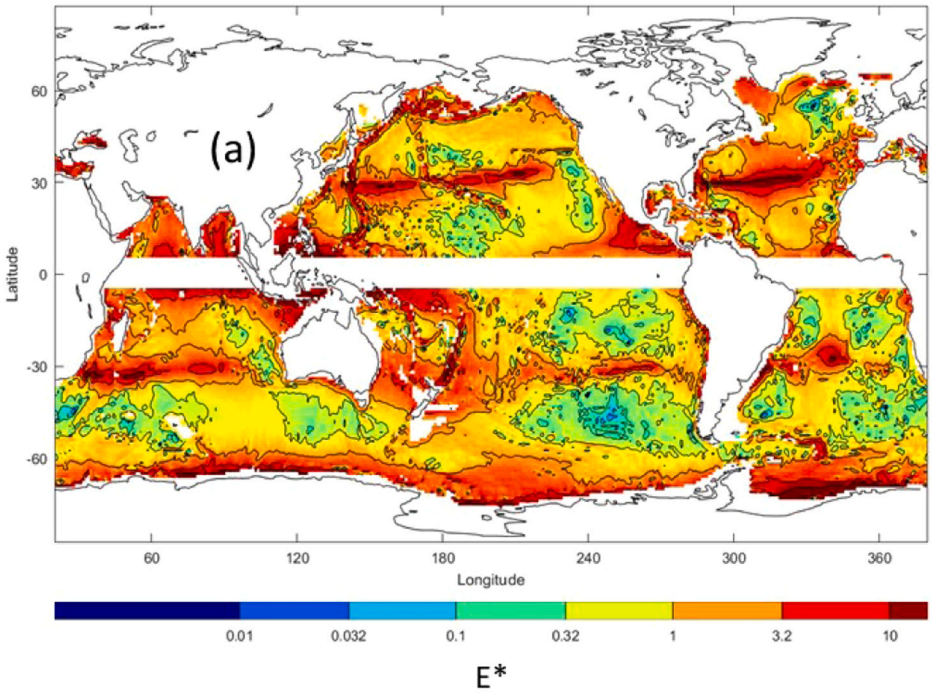

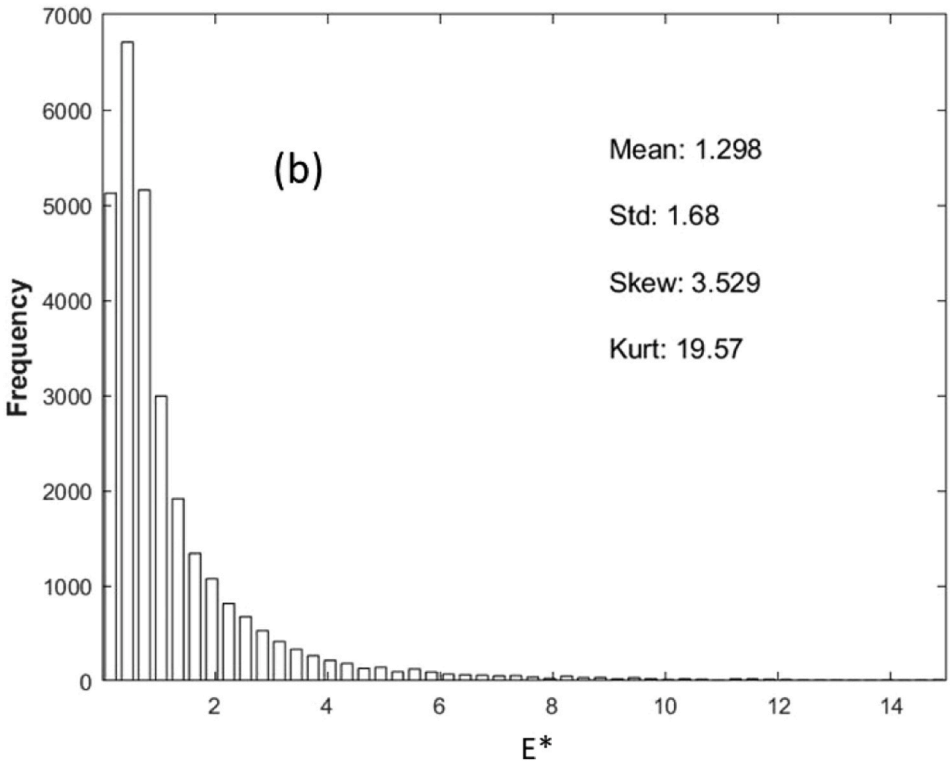

Fig. 6. Climatological annual mean non-dimensional E^*-number calculated using the COADS annual mean surface wind stress and the EIGEN-6C4 geoid undulation (N) data: (a) contour plot of E^*, (b) histogram of E^*.

distribution of E values (Fig. 4a). The histogram of E (Fig. 4b) indicates a positively skewed distribution with a long tail extending to values larger than 10. The statistical characteristics of E are 3.222 as the mean, 2.295 as the standard deviation, 0.9958 as the skewness, and 3.256 as the kurtosis.

8. Global Ekman transport with bottom

The bottom friction is a major damping mechanism on the effect of $\mathbf{g}_h$ to the Ekman transport [see (52b)]. With a linear relation of bottom velocity to estimate the friction [see (28)], a constant coefficient ($\gamma = 4 \times 10^{-6} \mathrm{ms}^{-1}$) is used [see (31)]. This coefficient might be appropriate for the basin-wide, deep, flat and open seas, but too weak for the shallow seas. Since the e-folding depth (d) of the buoyancy frequency is assumed 1.3 km [see (22a), (31)], the regions with water depth shallower than 1.3 km are excluded from the computation.

The calculated global Ekman transport has different patterns due to the surface wind stress $\mathbf{M}_W$ (Fig. 2a) and due to due to $\mathbf{g}_h$ with bottom ($\mathbf{M}_G^*$) (Fig. 5a). The intensities of the Ekman transport components $|\mathbf{M}_W|$ (Figure2b) and $|\mathbf{M}_G^*|$ (Fig. 5b) have different spatial distributions and strengths. The histogram of $|\mathbf{M}_W|$ (Fig. 2c) shows near Gamma distribution. However, the histogram of $|\mathbf{M}_G^*|$ (Fig. 5c) shows near Weibull distribution with the shape parameter of 1.5 and scale parameter of 10, and with the mean and standard deviation (1118, 1705) kg $\mathrm{m}^{-1}\mathrm{s}^{-1}$.

Importance of $\mathbf{g}_h$ on the Ekman transport with bottom is also shown in the world ocean distribution of E^* values (Fig. 6a). The histogram of E^* (Fig. 6b) indicates a positively skewed distribution with a long tail extending to values larger than 10. The statistical characteristics of E^* are 1.298 as the mean, 1.680 as the standard deviation, 3.529 as the skewness, and 19.57 as the kurtosis. the global mean Ekman transport is nearly the same order of magnitude due to $\mathbf{g}_h$ with bottom ($|\mathbf{M}_G^*|$) as due to the surface wind stress $|\mathbf{M}_W|$. Thus, $\mathbf{g}_h$ cannot be neglected in comparison to the surface wind stress in the Ekman layer dynamics.

Note that high value bands of E number (Fig. 4a) and E^*number (Fig. 6a) are located along 30°S, 30°N, and coast of Antarctic. This is due to the existence of low intensity bands of the traditional Ekman transport (i.e. due to wind stress) $|\mathbf{M}_W|$ in these locations (Fig. 2b). Also, the global mean is much smaller for E^*(1.298) than for E (3.222), which indicates the bottom friction damps the Ekman transport due to $\mathbf{g}_h$.

9. True-vertical coordinate versus deflected-vertical coordinate

As mentioned in the Introduction section, the true vertical direction $\mathbf{n}$ (upward positive) is with the true gravity $\mathbf{g}$,

$$\mathbf{g}(\lambda, \varphi, z) = -|\mathbf{g}(\lambda, \varphi, z)|\mathbf{n}(\lambda, \varphi, z) \tag{57}$$

The true horizonal surfaces are the equipotential surfaces of the true gravity. The geoid is one of them. On a true horizontal surface, the orthogonal unit vectors are represented by [$\mathbf{e}_1(\lambda,\varphi,z)$, $\mathbf{e}_2(\lambda,\varphi,z)$], but not ($\mathbf{i}$, $\mathbf{j}$). With such a true-vertical coordinate, the true gravity $\mathbf{g}$ has the vertical component only and no true-horizontal component. This treatment seems attractive to oceanography. However, it is not feasible at all since the unit vectors [$\mathbf{e}_1(\lambda,\varphi,z)$, $\mathbf{e}_2(\lambda,\varphi,z)$,$\mathbf{n}(\lambda,\varphi,z)$] vary at each point inside the oceans, and it is almost impossible to convert any ocean model (theoretical or numerical) with the standard gravity (-$g_0\mathbf{k}$) into the model with the true gravity $\mathbf{g}$ using the reference coordinates with the unit vectors [$\mathbf{e}_1(\lambda,\varphi,z)$, $\mathbf{e}_2(\lambda,\varphi,z)$,$\mathbf{n}(\lambda,\varphi,z)$]. The alternative treatment is to keep the deflected-vertical direction $\mathbf{k}$ and deflected-horizontal surface ($\mathbf{i}$, $\mathbf{j}$) as the same as the oceanographic tradition. With this treatment, the unit vectors ($\mathbf{i}$, $\mathbf{j}$, $\mathbf{k}$) are independent on (λ, φ, z). It is easy to replace the standard gravity (-$g_0\mathbf{k}$) by the true gravity $\mathbf{g}$ (= $\mathbf{g}_h$ -$g_0\mathbf{k}$) in any ocean models. Besides, the deflected-vertical coordinate system such as the polar spherical coordinate system (λ, φ, z) is widely used in all disciplines of geosciences such as the representation of the gravity model in geodesy.

10. Conclusion

The true gravity has latitudinal and longitudinal (i.e., deflected-horizontal) components ($\mathbf{g}_h$). Importance of $\mathbf{g}_h$ in the ocean Ekman transport with and without bottom is demonstrated in this study using the dynamic equation with the true gravity $\mathbf{g}(\lambda, \varphi, z)$. With the constant eddy viscosity K and the e-folding type depth-dependent buoyancy frequency (no deflected-horizontal density gradient), new formulae have been derived for the Ekman spiral and Ekman transport. The Ekman transports due to the surface wind stress ($\mathbf{M}_w$), due to $\mathbf{g}_h$ with no bottom ($\mathbf{M}_G$), and due to $\mathbf{g}_h$ with bottom ($\mathbf{M}_G^*$) are identified using the two independent datasets: COADS for the surface wind stress ($\boldsymbol{\tau}$), and EIGEN-6C4 geoid height (N) for $\mathbf{g}_h$. The global mean of the ratio is estimated as 3.222 between $|\mathbf{M}_G|$ and $|\mathbf{M}_w|$ (with no bottom) and as 1.298 between $|\mathbf{M}_G^*|$ and $|\mathbf{M}_w|$ (with bottom). Note that this result is only for the special conditions (constant K and e-folding near-inertial buoyancy frequency), not for the eddy viscosity and density in the real ocean. However, it demonstrates that the deflected-horizontal gravity component ($\mathbf{g}_h$) is an important forcing term in addition to the surface wind stress ($\boldsymbol{\tau}$) in the ocean Ekman layer dynamics. Since the Ekman dynamics or any ocean dynamics aim to describe and predict the real ocean, the deflected-horizontal gravity component ($\mathbf{g}_h$) needs to be included in numerical models for real oceans.

Finally, if the oceanographic community wants to keep the traditional terminology about the vertical (normal to the Earth sphere/ellipsoid) and horizontal (Earth spherical/ellipsoidal surface), the direction along the gravity vector $\boldsymbol{g}$ (= $\mathbf{i}g_\lambda$+ $\mathbf{j}g_\varphi$+ $\mathbf{k}g_z$) should be called the **true vertical**; and the equipotential surface such as the geoid should be called the **true horizontal**.

Declaration of Competing Interest

The authors declare that they have no known competing financial interests or personal relationships that could have appeared to influence the work reported in this paper.

Acknowledgements

The author thanks Mr. Chenwu Fan's outstanding efforts on computational assistance, the International Research Institute for Climate and Society for the COADS surface wind stress data, the International Centre for Global Erath Models (ICGEM) for the EIGEN-6C4 geoid height data, and the Dean of Research Office at the Naval Postgraduate School for paying the publication cost.

References

Cassinis, G., 1930. Sur l'adoption d'une formule international pour la pésanteur normale. Bull. Géodésique 26, 40–49.
Chu, P.C., 2015. Ekman spiral in horizontally inhomogeneous ocean with varying eddy viscosity. gravity in large scale ocean dynamics. Pure Appl. Geophys. 172, 2,831–2,857.
Chu, P.C., 2021. Ocean dynamic equations with the real gravity. Nature Sci. Rep. 11, 10 https://doi.org/10.1038/s41598-021-82882-1.
Chu, P.C., 2021. True gravity in atmospheric Ekman layer dynamics. Journal of Geophysical Research. https://doi.org/10.1029/2021JD035293.
da Silva, A., Young, A.C., Levitus, S., 1994. Atlas of Surface Marine Data, Volume 1: Algorithms and Procedures, number 6, ⟨https://www.nodc.noaa.gov/OC5/ASMD94/pr_asmd.html⟩.
Egbert, G.D., Ray, R.D., 2000. Significant dissipation of tidal energy in the deep ocean inferred from satellite altimeter data. Nature 405, 775–778.
Ekman, V.W., 1905. On the influence of the earth's rotation on ocean-currents. Ark. Mat. Astron. Fys. 2, 1–52.
Garrett, C., 2001. What is the 'near-inertial" band and why is it different from the rest of the internal wave spectrum? J. Phys. Oceanogr. 31, 962–971.
Gill, A.E., 1982. Atmosphere-ocean dynamics. In: Int. Geophys. Ser., 30. Academic Press, New York, pp. 91–94.
Hackney, R.I., Featherstone, W.E., 2003. Geodetic versus geophysical perspectives of the 'gravity anomaly'. Geophys. J. Int. 154, 35–43.
King, B., Stone, M., Zhang, H.P., Gerkema, T., Marder, M., Scott, R.B., Swinney, H.L., 2012. Buoyancy frequency profiles and internal semidiurnal tide turning depths in the oceans. J. Geophys. Res. 117, C04008 https://doi.org/10.1029/2011JC007681.
Kostelecký, J., Klokočnìk, J., Bucha, B., Bezděk, A., Förste, C., 2015. Evaluation of the gravity model EIGEN-6C4 in comparison with EGM2008 by means of various functions of the gravity potential and by BNSS/levelling. Geoinformatics FCE CTU, 14 (1), http://doi.org//10.14311/gi.14.1.1.
Moon, W., Tang, R., 1987. Ocean bottom friction coefficient from SEASAT-ALT data (Hudson Bay). Geophys. J. Int. 88, 535–567.
National Geospatial-Intelligence Agency, 1984. Department of Defense World Geodetic System 1984 (WGS84). Its definition and relationships with local geodetic systems. NIMA. TR8350.2., 3rd Edition, Eqs. 4–1.
Price, J.F., Weller, R.A., Schudlich, R.R., 1987. Wind-driven ocean currents and Ekman transport. Science 238, 1534–1538.
Sandwell, D.T., Smith, W.H.F., 1997. Marine gravity anomaly from Geosat and ERS 1 satellite altimetry. J. Geophys. Res. 102 (B5), 10,039–10,054.
Stacey, M.W., Pond, S., LeBlond, P.H., 1986. A wind-forced Ekman spiral as a good statistical fit to low-frequency currents in a coastal strait. Science 233, 470–472.
Vaníček, P., Krakiwsky, E., 1986. Geodesy The Concepts. Part 5 Earth Gravity Field 1986 North-Holland Amsterdam 457 581.
Vallis, G.K., 2006. Atmospheric and Oceanic Fluid Dynamics, First ed. Cambridge University Press, Cambridge, pp. 55–57.